Cold-Sprayed AZ91D Coating and SiC/AZ91D composite coatings

Y. Wang, B. Normand, X. Suo, M.-P. Planche, H. Liao, J. Tang

coatings

MDPI

Article

Cold-Sprayed AZ91D Coating and SiC/AZ91D Composite Coatings

Yingying Wang [1], Bernard Normand [2], Xinkun Suo [3,*], Marie-Pierre Planche [4], Hanlin Liao [4] and Junlei Tang [1,*]

1 College of Chemistry and Chemical Engineering, Southwest Petroleum University, Chengdu 610500, China; yingyingwanglyon@126.com
2 Université de Lyon, INSA de Lyon, MATEIS CNRS UMR 5510, 69621 Villeurbanne, France; bernard.normand@insa-lyon.fr
3 Key Laboratory of Marine Materials and Related Technologies, Key Laboratory of Marine Materials and Protective Technologies of Zhejiang Province, Ningbo Institute of Materials Technology and Engineering, Chinese Academy of Sciences, Ningbo 315201, China
4 ICB UMR 6303, CNRS, University Bourgogne Franche-Comté, UTBM, 90100 Belfort CEDEX, France; marie-pierre.planche@utbm.fr (M.-P.P.); hanlin.liao@utbm.fr (H.L.)
* Correspondence: suoxinkun@gmail.com (X.S.); tangjunlei@126.com (J.T.); Tel.: +86-158-2557-3811 (X.S.); +86-186-0803-9391 (J.T.)

Received: 21 January 2018; Accepted: 23 March 2018; Published: 26 March 2018

Abstract: As an emerging coating building technique, cold spraying has many advantages to elaborate Mg alloy workpieces. In this study, AZ91D coatings and AZ91D-based composite coatings were deposited using cold spraying. Coatings were prepared using different gas temperatures to obtain the available main gas temperature. Compressed air was used as the accelerating gas, and although magnesium alloy is oxidation-sensitive, AZ91D coatings with good performance were obtained. The results show that dense coatings can be fabricated until the gas temperature is higher than 500 °C. The deposition efficiency increases greatly with the gas temperature, but it is lower than 10% for all coating specimens. To analyze the effects of compressed air on AZ91D powder particles and the effects of gas temperature on coatings, the phase composition, porosity, cross-sectional microstructure, and microhardness of coatings were characterized. X-ray diffraction and oxygen content analysis clarified that no phase transformation or oxidation occurred on AZ91D powder particles during cold spraying processes with compressed air. The porosity of AZ91D coatings remained between 3.6% and 3.9%. Impact melting was found on deformed AZ91D particles when the gas temperature increased to 550 °C. As-sprayed coatings exhibit much higher microhardness than as-casted bulk magnesium, demonstrating the dense structure of cold-sprayed coatings. To study the effects of ceramic particles on cold-sprayed AZ91D coatings, 15 vol % SiC powder particles were added into the feedstock powder. Lower SiC content in the coating than in the feedstock powder means that the deposition efficiency of the SiC powder particles is lower than the deposition efficiency of AZ91D particles. The addition of SiC particles reduces the porosity and increases the microhardness of cold-sprayed AZ91D coatings. The corrosion behavior of AZ91D coating and SiC reinforced AZ91D composite coating were examined. The SiC-reinforced AZ91D composite coating reveals higher corrosion potential than magnesium substrate; therefore, it serves as a cathode for the magnesium substrate, the same as the AZ91D coating on magnesium substrate. As the SiC powder is semi-conductive, the embedded SiC particles reduce the electrochemical reaction of the AZ91D coating. The addition of SiC particles increases the corrosion potential of the coating, meanwhile increasing the galvanic potential and decreasing the negative galvanic current of the coating-substrate couple.

Keywords: cold spraying; coating; magnesium alloy; composite coatings; corrosion; microstructure

1. Introduction

Magnesium (Mg) alloys have potential use in aircraft and automobile industries due to their excellent specific strength [1]. They are also used to protect steel structures from corrosion in freshwater and soil environments as sacrificial anodes [2]. Casting is the main technique to produce AZ91D alloy workpieces; however, it is not suitable to fabricate large or complex-shaped products [3]. In addition, AZ91D work pieces are difficult to be repaired using traditional techniques (tungsten inert gas (TIG) welding [4], metal inert gas (MIG) welding [5], and thermal spraying [6], etc.) due to their high-temperature activity.

As an emerging coating building and rebuilding technique, cold spraying has advantages to elaborate Mg alloy workpieces [7,8]. In cold spraying, particles are accelerated to a high velocity (300~1200 $m \cdot s^{-1}$) by a high-pressure thermal gas through a de Laval-type nozzle. Then, the particles can deposit onto a substrate and form a coating once the particle velocity exceeds the critical velocity of the material [9,10]. In the view of bonding, the jet formation of impact couples is viewed as the necessary condition.

In cold spraying, the main gas temperature is lower than the melting point of the sprayed material; thus, oxidization can be avoided. In the past decade, cold spraying has been used to deposit oxidation-sensitive alloys, such as Ti [11], Al [12,13], and Mg [8] alloy coatings. In addition, cold spraying was successfully used to repair Al alloy gearbox components [14]. However, few publications on cold-sprayed AZ91D coatings and AZ91D-based composite coatings were reported. Based on this fact, AZ91D powder was used to elaborate coatings using cold spraying in this paper, and SiC powder was used as reinforcing particles to deposit the composite coatings. In consideration of the application of cold-sprayed Mg alloy workpieces, compressed air, not noble gas, was used as the accelerating gas. Different gas temperatures were conducted to study the feasibility of fabricating cold-sprayed Mg alloy work pieces, and then ceramic particles were added as reinforcement to improve the performance of the coatings. The effects of gas temperature and the addition of ceramic particles on the coatings' microstructure and electrochemical behaviors were evaluated.

2. Materials and Methods

2.1. Materials

A commercially-available AZ91D powder (WeiHao Magnesium Powder Co., Ltd., Tangshan, China) and SiC powder (Sulzer Metco, Bron, France) were used to produce coatings. The AZ91D particles presented a spherical shape (Figure 1a), and the grain orientation is random (Figure 1b). SiC particles show dendritic morphology with sharp edges (Figure 1c). Size distribution of the powder was examined using a MASTERSIZER 2000 system (Malvern Panalytical Ltd., Royston, UK). The size distribution of the AZ91D powder was in the range from 34 μm to 81 μm, and averaged 52 μm (Figure 1d). The size distribution of SiC powder is from of 4 μm to 55 μm, and averaged 15 μm (Figure 1e). The content of SiC particles in the feedstock powder was 30 vol %. Stainless steel and magnesium plates with a dimensions of 60 mm × 20 mm × 2 mm were used as substrates. The substrates were sandblasted using alumina grits (ISO 6344, Grit designation, P100) prior to spraying.

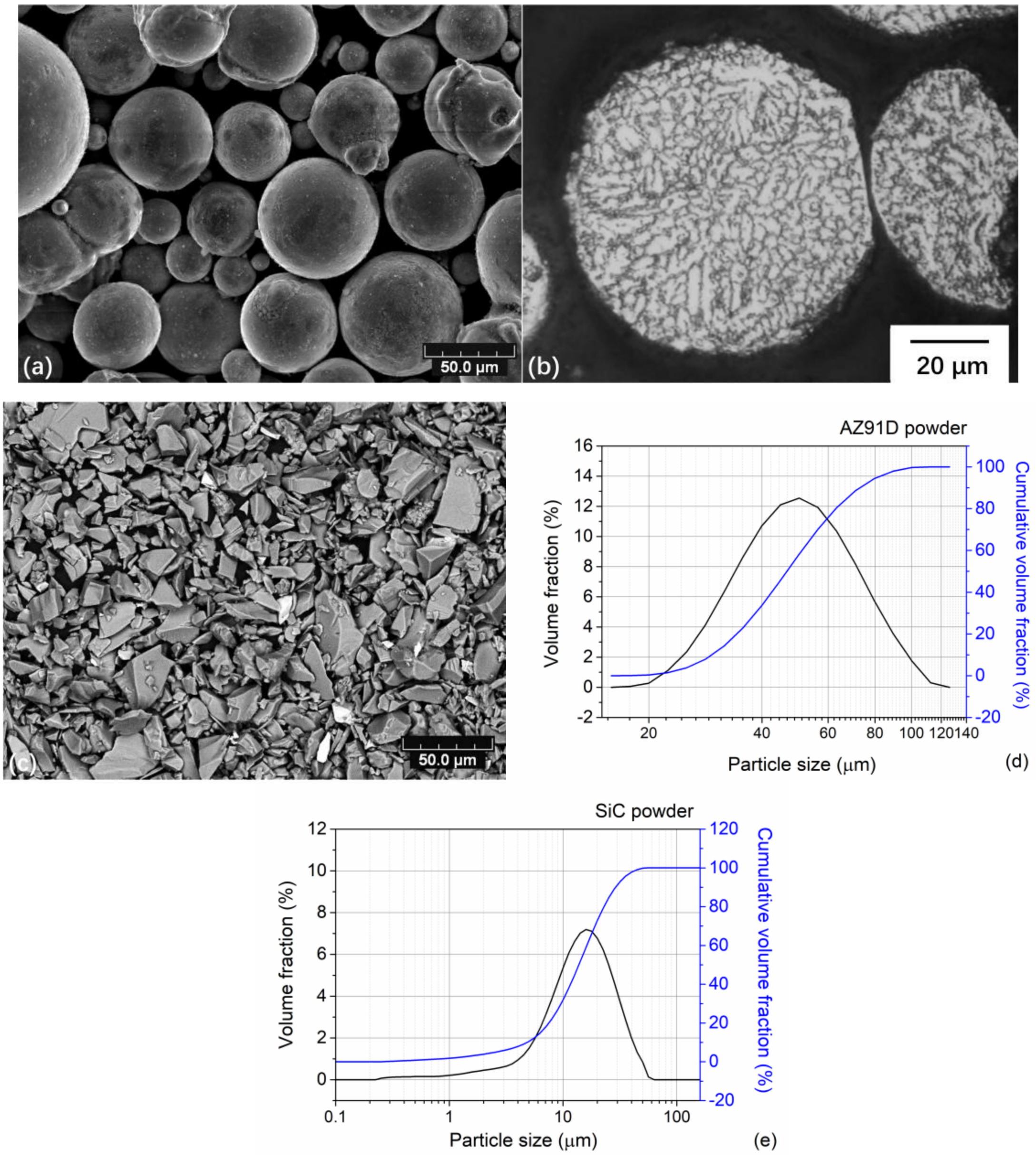

Figure 1. Morphology of the original AZ91D powder (**a**); sectional microstructure of an AZ91D particle after etching (**b**); and the morphology of SiC powder (**c**). Size distribution of the AZ91D powder particles (**d**) and SiC powder particles (**e**).

2.2. Spraying Conditions

A self-designed rectangular cross-section nozzle was used to fabricate the coatings. The expansion ratio of the nozzle is 4.9. The outlet diameter of the nozzle is 6.5 mm and the divergent section length is 170 mm. Compressed air and argon were used as the main gas and the carrier gas, respectively. The main gas pressure in a pre-chamber was 2.5 MPa, and the gas temperatures were changed in a range from 450 °C to 600 °C. The powder feed rate was 70 g·min^{-1}. The standoff distance was 30 mm. The nozzle was fixed on a robot in order to maintain a traverse speed of 100 mm·s^{-1}. The beam distance was 2 mm. Each coating contains two layers.

2.3. Coating Characterization

The particle morphology and coating fracture morphologies were observed using a scanning electron microscope (SEM) (JEOL, JSM-5800LV, Tokyo, Japan). The coatings cross-sections were observed using an optical microscope (OM) (Nikon, Tokyo, Japan) and SEM. Porosity was estimated using an open software, Image J (National Institutes of Health, Bethesda, MD, USA). X-ray diffraction (XRD, D/mas-2400, Rigaku, Tokyo, Japan) was used to determine the phases in the feedstock powder and coatings. Oxygen contents in both the feedstock powder and cold-sprayed coatings were measured using an oxygen, nitrogen, and hydrogen analyzer (ONH-2000, ELTRA, Haan, Germany). The microhardness of the coatings was measured under a load of 300 g with a dwell time of 15 s. For each coating, three specimens were used to measure the microhardness. In addition, for each specimen, 10 measurements were conducted in random locations to obtain the average microhardness.

To evaluate the corrosion protective effects of the Mg alloy coatings, electrochemical measurements were performed by a standard three-electrode electrochemical cell in air saturated with a 0.1 M Na_2SO_4 solution. Coating specimens were conducted as the working electrode with a surface of 10 mm × 10 mm. The counter electrode was a platinum sheet with a surface of 8 mm × 8 mm. The reference electrode was a saturated mercury sulfate electrode (Hg/Hg_2SO_4). The solution concentration inside the reference electrode compartment was a saturated K_2SO_4 solution, with a potential of 640 mV with respect to the normal hydrogen electrode (NHE) and a potential of 400 mV with respect to the saturated calomel electrode (SCE). The open circuit potential (OCP) and polarization scans were conducted on an electrochemical workstation (Reference 600TM, Potentiostat/Galvanostat/ZRA, Gamry Instruments, Inc., Warminster, PA, USA). Potentiodynamic scans were performed from −0.1 V to 2.5 V (vs. OCP) with a scan rate of 1 mV/s. Galvanic interaction between the coatings and the substrate has been studied by continuous monitoring of the galvanic potential and the galvanic current using ZRA measurements.

3. Results

3.1. Effects of Gas Temperature on the AZ91D Coatings

The microstructures of the coatings elaborated at 500 °C, 550 °C, and 600 °C are shown in Figure 2a–c, respectively. It was found that the coating could be built on stainless steel until the main gas temperature increased to 500 °C. It is reported that in cold spraying the particle velocity increases as the main gas temperature increases. Thus, it can be deduced that the particle velocity was lower than the critical velocity of magnesium when the main gas temperature was lower than 500 °C. The critical velocity of Mg was reported in a range of 653 m/s to 677 m/s, which was calculated by simulation [8]. The particle velocity increased higher than the critical velocity as main gas temperature is higher than 500 °C; thus, coatings could be built.

In Figure 2, the part between the dark region on the top and the uniform gray area at the bottom is the coating. The thickness increases with the gas temperature as the average coating thickness is 177.2 ± 30.7, 482.8 ± 69.5, and 516.5 ± 50.4 µm when the gas temperature is 500 °C, 550 °C, and 600 °C. No visible micro–channels in the entire view of section can be observed for all coating specimens. At the coating/substrate interface, there are neither cracks nor delamination. The coatings reveal a dense microstructure. Several dark dots are identified as pores. The AZ91D powder particles are fully deformed as the original spherical shape can no longer be recognized. The gains of the AZ91D powder particles are elongated along the direction vertical to their impacting direction.

Figure 3 shows the analysis of the grain in a projected and bounced particle on the substrate. The white arrow indicates the direction of impact on the particle. It was found that not only the shape of the particles changes, but also the orientation of the grains. Within the original particle, the grain orientation is random. After impact, an ordered arrangement in the impact zone is presented and the grain arrangement direction is perpendicular to the direction of the rebound. As a result, AZ91D powder particles can deform and form a cold-sprayed coating although it is difficult to deform.

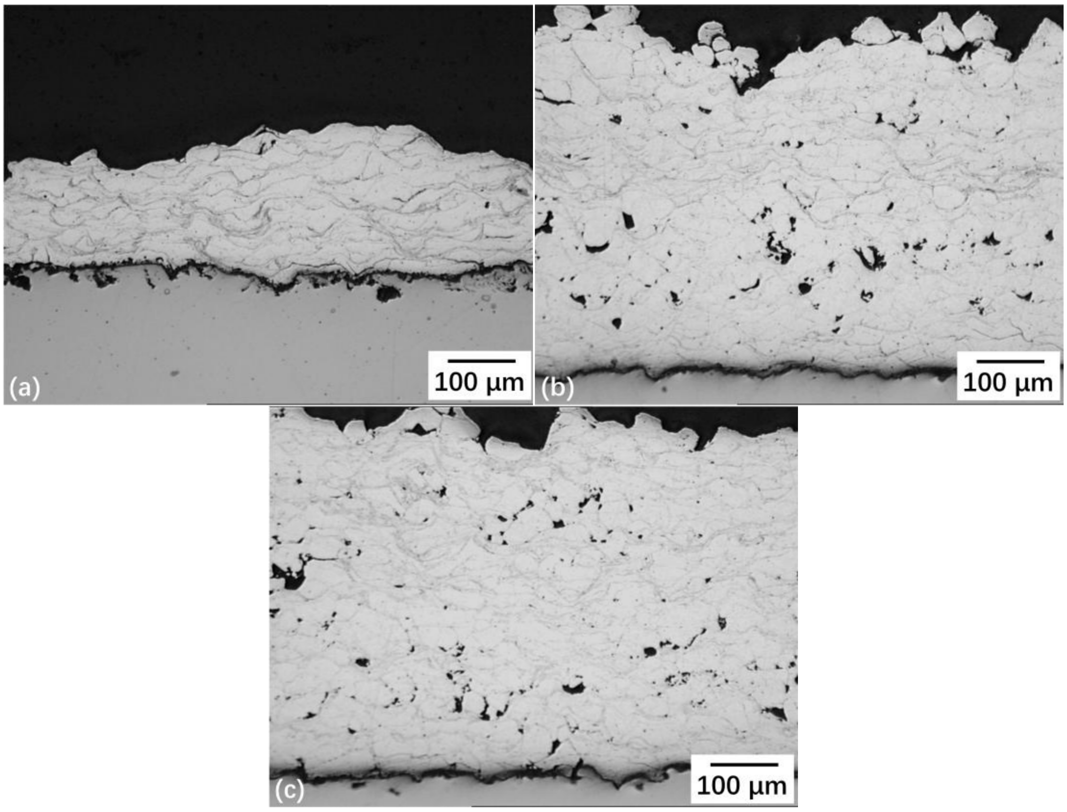

Figure 2. Microstructures of coatings deposited at 500 °C (**a**), 550 °C (**b**), and 600 °C (**c**).

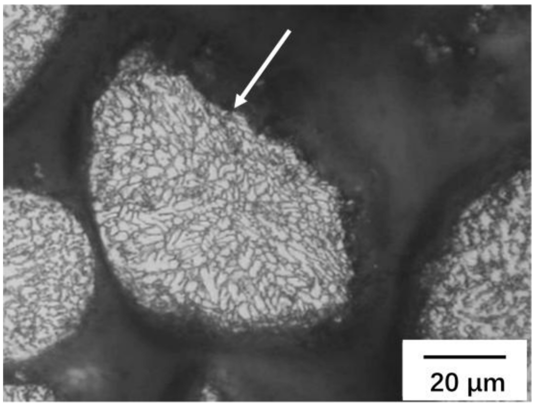

Figure 3. Morphology of a particle after the rebound.

The coating porosities were calculated. The average porosities were 3.9% (±0.7%), 3.6% (0.6%), and 3.7% (0.1%) when the gas temperature was 500 °C, 550 °C, and 600 °C, respectively. It is found that coating porosity decreased with an increase in the main gas temperature. In this study, main gas temperatures were restricted in a narrow range: on one hand, it must ensure particle deposition; on the other hand, it should be lower than the melting point of the AZ91D particles. The narrow temperature interval resulted in a narrow particle velocity range which, in turn, resulted in the slight variation of the porosities. Additionally, the porosity of the AZ91D coating is close to the porosity of the pure magnesium coating [7]. When compared with another widely-used sacrificial coating, i.e., aluminum alloy (the porosity is 1~2%), it is slightly larger [12,15].

The effects of gas temperature on the deposition efficiency of cold-sprayed AZ91D coatings are presented in Figure 4. At 450 °C, no coatings were obtained. From 500–600 °C, deposition efficiency increases with gas temperature. The deposition efficiency is low, which is lower than 10% for all specimens at different gas temperature. This means the AZ91D alloy is difficult to deposit using the cold spraying conditions in this study. Thanks to the recyclability of feedstock powder in cold spraying, we consider that the deposition efficiency would not restrict the application of cold-sprayed Mg alloy workpieces. Moreover, we have obtained high deposition efficiency for pure magnesium, whose deposition efficiency is approximately 60% at 600 °C [7]. The difference in deposition efficiency could be due to the different original shape of powder particles. In [7], the pure magnesium powder particles show an irregular shape instead of a spherical shape. It is reasonable to envisage the possibility of a higher deposition efficiency. When compared with the other materials in the literature, because of the weaker plastic deformation ability, the deposition efficiency is lower than that of cold-sprayed aluminum coatings deposited under similar conditions [16]. The gas temperature is 400 °C and 500 °C, and the gas pressure is 2.1–2.9 MPa in [16]. The deposition efficiency is even lower than that of cold-sprayed titanium alloy [12], however, the gas pressure is much higher, which is 4 MPa, as reported.

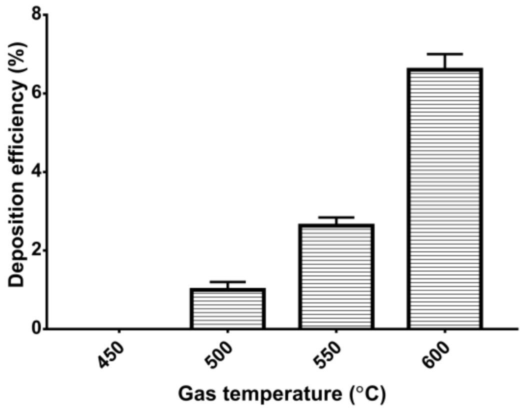

Figure 4. Deposition efficiency of AZ91D coatings deposited at different gas temperatures.

XRD and oxygen content analysis were employed to evaluate the phase transformation and oxidization of the particles during cold spraying. XRD patterns of the powder particles and coatings are shown in Figure 5. It can be found that there were only Mg and $Mg_{17}Al_{12}$ phases in the coatings, which were the same as those in the original particles. This allows the conclusion that there was no reaction or phase transformation during cold spraying [17,18]. Another interesting phenomenon was the peak intensity evolution of Mg before and after spraying. The peak intensity of crystal plane (0002) in the coatings obviously increased compared to that in the powder original. This may be due to the texture caused by the plastic deformation of the particles during impact [19]. Similar phenomena were also found in pure Mg coatings fabricated using cold spraying [8]. The texture depends on the deformation rate and velocity. In cold spraying, a typical particle/substrate contact time was 40 ns [20]. The intensive deformation happened during this time at a high velocity. Therefore, the deformation texture occurred.

The result of oxygen content analysis shows that the oxygen content in the coating produced at 600 °C (273 ± 55 ppm) was similar to the value in the original particles (200 ± 107 ppm). The in-flight time of Mg particles in the nozzle was less than 1 ms; additionally, the main gas temperature was lower than the melting point of the material. Therefore, the coatings did not undergo deterioration or oxidization. This is the same in cold-sprayed pure magnesium coating. The oxygen content of the Mg coating deposited at 630 °C is reported as 229 ± 124 ppm, which is much lower than the oxygen content of original Mg powder (866 ± 122 ppm). The decrease of oxygen content benefits from the fragmentation of the oxide film of the Mg particles. During cold spraying, the oxide film of the particles can be broken up, and metallurgical bonding could be achieved. Therefore, a higher particle velocity induced by a higher main gas temperature could result in a greater fragmentation of the oxide film. From the oxygen content results, the possibilities of the oxide film breaking up is much smaller for AZ91D powder particles in this study.

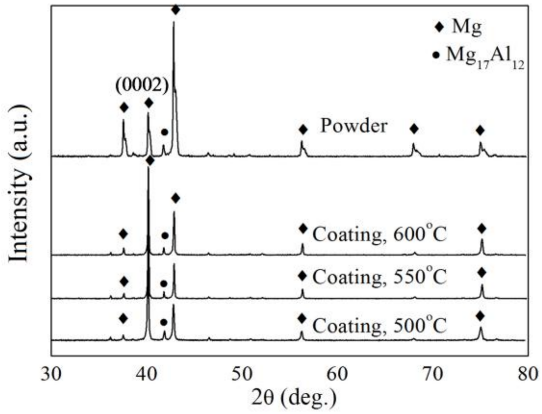

Figure 5. XRD patterns of AZ91D powder and AZ91D coatings deposited at different temperatures.

The fracture morphologies of the coatings elaborated at 500, 550, and 600 °C are shown in Figure 6. Deformed particles can be found everywhere in Figure 6a. No ductile fracture features can be found in this image. Therefore, the deposition of AZ91D coatings fabricated at 500 °C could be mainly due to the mechanical interlocking and jet mixing. An obvious laminar manner could be observed in the fracture surfaces. This is evidence of the plastic deformation.

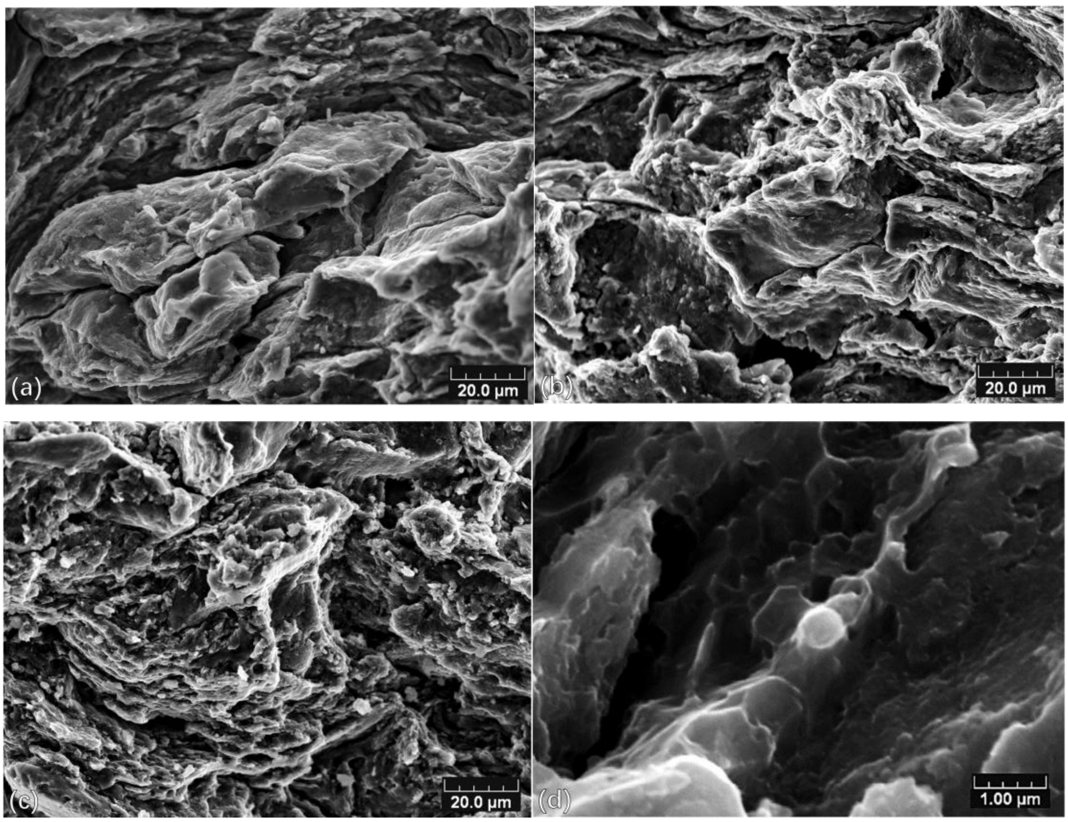

Figure 6. Fracture microstructures of AZ91D coatings elaborated at 500 °C (**a**), 550 °C (**b**), 600 °C (**c**); and partial enlarged drawing in **b** (**d**).

A partial enlarged image of Figure 6b is shown in Figure 6d. Dimple structures can be observed. The impact melting was found in many impact couples, especially in the impact of Al-based materials due to their low melting point. The melting point of AZ91D particles is lower than Al; thus, impact melting possibly occurred. According to the modeling result, the interfacial temperature of the impact couples could be close to the melting point of the impact materials [18]. The particle velocity increased as the main gas temperature increased to 550 °C; thus, some particles had more kinetic energy to achieve a higher deformation and, consequently, resulted in a higher interface temperature. This contributed to the partial impact melting between AZ91D particles. However, the dimple structures were very few. Therefore, the impact melting did not play a key role in bonding. The bonding mechanism of the coating is mainly the mechanical interlocking. It can be estimated that the bond of the coating and the substrate or between the particles is weak.

The microhardness of the AZ91D coatings elaborated at different temperatures was measured, and the result is shown in Figure 7. The microhardness of the coatings was about 100 HV, which was lower than the stainless steel substrate, but higher than the microhardness of as-casted bulks, which is 63.7 HV as reported by Masaki Sumida [21]. This is due to the work-hardening effect of subsequent particles during cold spraying. The same phenomenon was also found in cold-sprayed Al coating, Cu coating, and Fe coating [22].

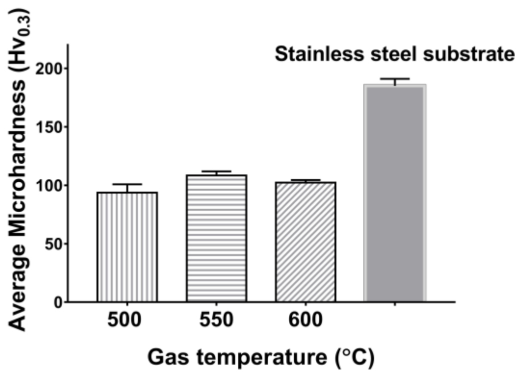

Figure 7. Microhardness of AZ91D coatings deposited at different temperatures.

Less dense coating with higher porosity results in lower microhardness. It can also be found that the microhardness of the coatings did not vary obviously as a function of the main gas temperature. This is due to the similar coating porosity in the narrow gas temperature range. Moreover, the microhardness of the AZ91D coating is much higher than the Mg coating using the same cold spraying conditions. The microhardness of the cold-sprayed Mg coating is approximately 38 HV [8].

3.2. Effects of Ceramic Particles Addition on AZ91D Coatings

AZ91D and SiC/AZ91D composite coatings were produced on a magnesium substrate to study the effects of ceramic particles addition. Similar to the AZ91D coating, the as-sprayed SiC/AZ91D composite coating exhibited a relatively rough outer surface. Figure 8a,b shows the top surface morphology of the AZ91D coating and SiC/AZ91D composite coating. The majority of particles on the top layer adhere well. Crevices could be detected beside loosely-adhered particles. The porous top layer is formed due to the absence of a tamping effect of the next incoming particles. SiC particles can be easily found on the top surface, and which are randomly distributed.

The entire thickness of SiC/AZ91D composite coating is presented in Figure 8c. The coating reveals a fully-dense microstructure. SiC particles and a small quantity of pores are distributed homogeneously within the coating. The AZ91D particles are fully deformed, and the original spherical shape cannot be identified any more. SiC particles keep the irregular morphology as before the cold spraying process. Due to the good adhesion between the coating and the substrate, the interface is difficult to detect.

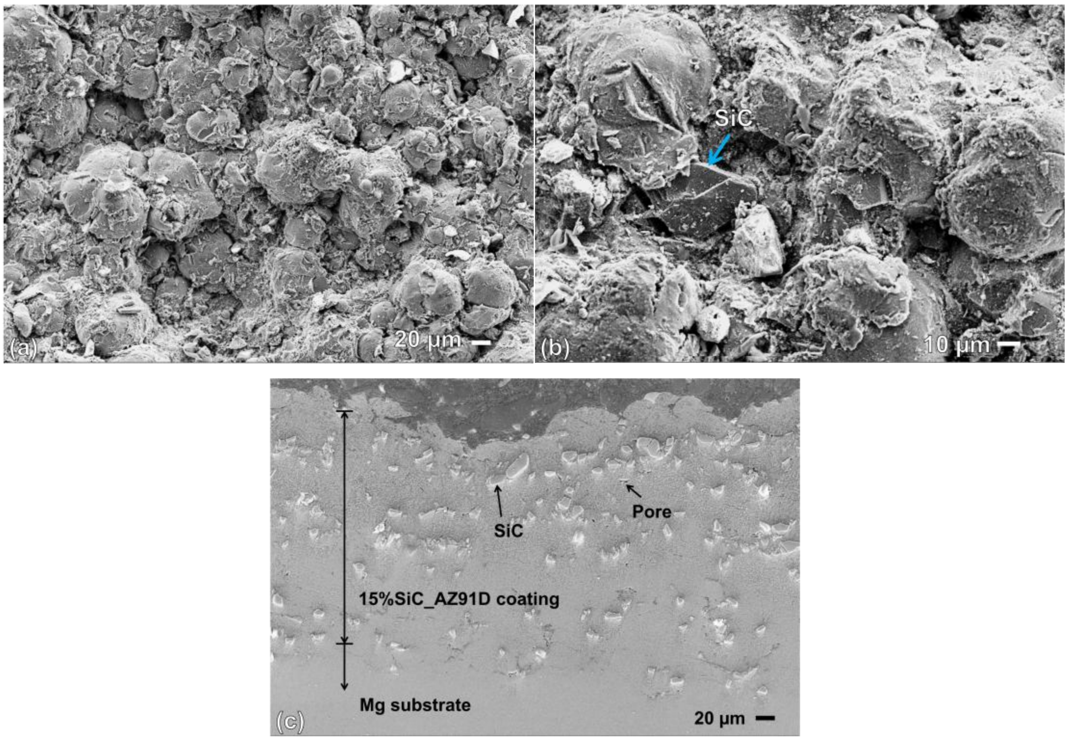

Figure 8. Top surface morphology the AZ91D coating (**a**), and SiC/AZ91D composite coating (**b**); and the cross–sectional microstructure SiC/AZ91D composite coating (**c**).

The result of the image analysis shows that the content of SiC powder particles is 10.7 ± 3.2 vol %, which is lower than the SiC content in the feedstock blended powder. It is deduced that the deposition efficiency of the SiC powder particles is lower than the deposition efficiency of AZ91D particles. The same result was found in the literature [13,23] in which the SiC content in feedstock is 30 vol %, while in the composite coating, the SiC content is less than 30%.

The porosity and microhardness were measured on the SiC/AZ91D composite coating. The porosity of the composite coating is 1% (±0.14%), and the microhardness is 139 HV (±16.7 HV). The addition of SiC particles involve a significant coating densification and increasing microhardness. The coating porosity decreases with SiC addition during spraying. On one hand, the addition of SiC particles increases the deformation of the AZ91D powder particles, so that the porosity of the composite coatings becomes lower than that of the AZ91D coating due to the peening effects of the SiC particles. On the other hand, the different morphologies and sizes of the Al 5056 matrix powders and mixed SiC particles also play an important role. The microhardness of the composite coating increased greatly compared with that of the AZ91D coating, which should also be attributed to the reinforcing effect of SiC particles and work hardening effect of cold spraying. The uniformly distributed SiC particles could restrict the deformation of the AZ91D matrix. Additionally, the dislocation tangle resulting from the working-hard effect will make the deformation of the matrix more difficult.

The OCP values monitored over 24 h for the AZ91D coating and the SiC/AZ91D composite coating, as well as the magnesium substrate, are shown in Figure 9a. Obviously, the potential of magnesium immersed in this medium is low. This is why magnesium is always used as a sacrificial anode to protect metal installations. Both coatings show higher potential than the magnesium substrate. It is, thus, demonstrated that the intermetallic compound $Mg_{17}Al_{12}$ does not intervene in corrosion mechanisms after 24 h of immersion. The composite coating has a significant nobler potential. The densification effect related to the presence of hard SiC particles limits the microcavities involving in the crevice corrosion initiation [13], which facilitates the formation of the MgO oxide film.

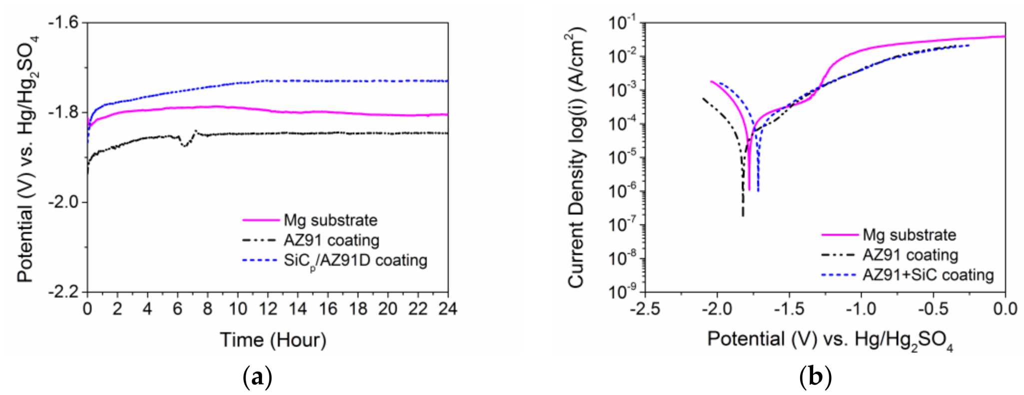

Figure 9. Corrosion characters for cold-sprayed AZ91D coating and SiC/AZ91D composite coating: open circuit potentials (**a**), and potentiodynamic polarization curves (**b**).

Figure 9b shows the polarization curves of the coatings compared to that of the substrate. These polarization curves complete the corrosion potential measurements that give the thermodynamic criteria only. Each range of the polarization curves gives information on the kinetics and the nature of the reactions that take place at the interfaces. The ranking of the corrosion potentials is the same as for Figure 9a. The corrosion potential of the Mg substrate is the same as the potential of the AZ91D coating. It is close to -1.9 V/Hg/Hg_2SO_4. For the composite coating this value is nobler and close to -1.75 V/Hg/Hg_2SO_4.

For potential values lower than the corrosion potentials, the polarization curves have the same trends and the same slopes. The recorded phenomena are identical. This is due to the reduction of hydrogen. Since the involved reactions are carried out by charge transfer, no diffusion of dissolved oxygen contribution is recorded. The significant difference in all electrochemical behaviors occurs for the anodic branch of the electrochemical behavior of the materials, for the nobler potentials, located after the corrosion potential. The substrate has a slight passive domain between -1.9 to -1.5 V/Hg/Hg_2SO_4, for which the current is relatively low. Beyond -1.5 V/Hg/Hg_2SO_4, the current density increases significantly to reach a diffusion plateau relative to the generalized corrosion of Mg. This polarization curve indicates two points: (i) interest of the polarization curves that permit to indicate the corrosion mode of metallic materials and (ii) Mg is very reactive in this medium. Indeed, if the AZ91D corrosion potential is identical to that of Mg, it should be noted that its electrochemical behavior in the anodic domain is very different. The shape of the curve is essentially the same as that of Mg, which is normal since the main element of AZ91D is magnesium. However, the current densities are much lower. This result is due to the presence of aluminum in the alloy and also to the coating morphology which has no porosity. This porosity could, indeed, show localized corrosion phenomena by the effect of cracks, which would be characterized by significant current densities increasing. The kinetics recorded for this coating is closed to that recorded for a passivated coating, thus, it is less reactive than the substrate. The electrochemical behavior of the composite coating is identical to that of the coating prepared with AZ91D alone. The addition of SiC powder particles does not affect the electrochemical behavior of the AZ91D coating, it only contributes to the densification of the coatings, which had already been demonstrated in a previous study dedicated to another sacrificial system [12].

Measurements using a zero resistance ammeter device were undertaken to analyze the galvanic couplings between the substrate and the coatings. These measurements give results to the mixed potential and the mixed current of the galvanic coupling. These results are presented in Figure 10. The measurements were carried out for 50 h. The mixed potential measured between AZ91D and the substrate is identical to that of the two materials, measured separately. The potential difference between these two elements is close to zero, which explains the value of the potential obtained, and which also explains why the galvanic current recorded for this AZ91D-Mg substrate system is close to zero, too. The AZ91D coating and the magnesium substrate show similar corrosion potentials in polarization tests, which results in a difficulty of predicting the polarity of this galvanic couple. The direction of galvanic current ensures that AZ91D coating is nobler than the magnesium substrate. The couple of SiC/AZ91D coating-Mg substrate shows higher galvanic potential and more negative galvanic current than the couple of AZ91D coating-Mg substrate. The mixed potential of the SiC/AZ91D-Mg substrate is driven by the potential of coating which was presented in Figure 10. The addition of SiC powder particles increase the absolute value of galvanic current, i.e., the SiC/AZ91D coating is nobler than the AZ91D coating on the Mg substrate.

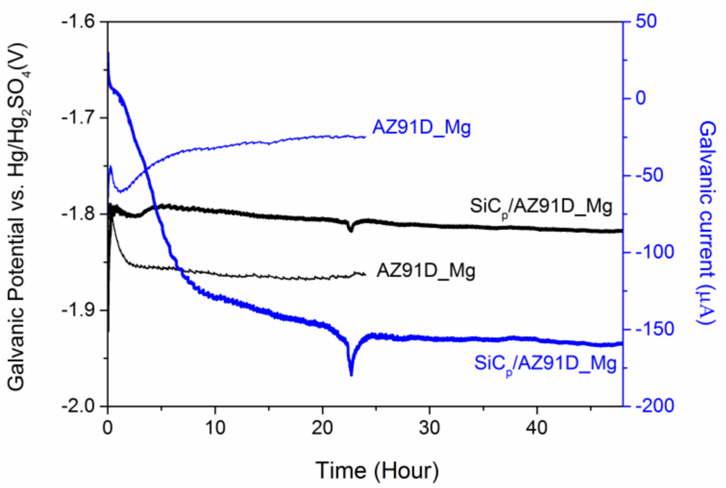

Figure 10. Time behavior of galvanic potential and galvanic current for the AZ91D coating and the SiC/AZ91D composite coating coupled to the magnesium substrate.

Electrochemical measurements confirm that, in both cases recorded in Figures 9 and 10, the behavior of the coatings controls the electrochemical behavior of the AZ91D-Mg system with or without SiC. In the case of an AZ91D coating, the galvanic coupling will not be effective because the potential difference and the galvanic current are close to zero. In the case of a SiC/AZ91D-Mg coating, the measurements indicate that when the composite coating is used to protect the Mg substrate, the galvanic coupling does not exist since the porosity is low. The addition of SiC during the spraying makes it possible to densify the coating and, thus, to avoid the connective porosity through the substrate.

4. Conclusions

AZ91D coatings and SiC-reinforced AZ91D composite coating were fabricated using cold spraying. Compressed air was used as the main gas, and the effects of gas temperature were studied. It was found that the gas temperature should be higher than 450 °C for cold spraying of spherical AZ91D powder particles. The deposition efficiency increases greatly with the gas temperature and it is lower than 10% for all coating specimens. The coating average porosity remained between 3.6% and 3.9% when the gas temperature is in the range of 500~600 °C. Coatings are denser when the gas temperature is higher. XRD results showed that no phase transformation or oxidization occurred during the cold spraying process of AZ91D. The microhardness of the coatings (approximately 100 HV) was much higher than that of as-casted bulks due to the work hardening effect. Gas temperature does not show an obvious influence on microhardness. Partial impact melting was found between AZ91D particles in the coatings fabricated at 550 °C and 600 °C.

15 vol % SiC powder particles were added to feedstock powder as reinforcement to improve the coating performance. Results showed that the SiC content of coatings is 10.7 ± 3.2 vol %. Reduced SiC content means that the deposition efficiency of the SiC powder particles is lower than the deposition efficiency of the AZ91D particles. The addition of SiC particles reduces the porosity and increases the microhardness of cold-sprayed AZ91D coatings. Both the AZ91D coating and SiC-reinforced AZ91D composite coating serve as the cathode for the magnesium substrate due to the relatively higher corrosion potential. The addition of SiC particles increases the open circuit potential of the AZ91D coating, meanwhile increasing the galvanic potential and decreasing the negative galvanic current of the coating-substrate couple.

Acknowledgments: This investigation is financially supported by the National Natural Science Foundation of China under grant no. 51601158 and the Qihang Science Research Foundation of Southwest Petroleum University, no. 2015QHZ013.

Author Contributions: X.S., M.P., and H.L. conceived and designed the experiments; Y.W. and X.S. performed the experiments; X.S., Y.W., and J.T. analyzed the data; B.N., M.P., and H.L. contributed materials; J.T. contributed analysis tools; and Y.W., X.S., and B.N. wrote the paper.

Conflicts of Interest: The authors declare no conflict of interest.

References

1. Esmaily, M.; Svensson, J.E.; Fajardo, S.; Birbilis, N.; Frankel, G.S.; Virtanen, S.; Arrabal, R.; Thomas, S.; Johansson, L.G. Fundamentals and Advances in Magnesium Alloy Corrosion. *Prog. Mater. Sci.* **2017**, *89*, 92–193. [CrossRef]
2. Liu, F.; Zhang, J.; Sun, C.; Yu, Z.; Hou, B. The Corrosion of Two Aluminium Sacrificial Anode Alloys in SRB-containing Sea Mud. *Corros. Sci.* **2014**, *83*, 375–381. [CrossRef]
3. Lun Sin, S.; Dubé, D.; Tremblay, R. An Investigation on Microstructural and Mechanical Properties of Solid Mould Investment Casting of AZ91D Magnesium Alloy. *Mater. Charact.* **2008**, *59*, 178–187. [CrossRef]
4. Kocurek, R.; Adamiec, J. The Repair Welding Technology of Casts Magnesium Alloy QE22. *Solid State Phenom.* **2013**, *212*, 81–86. [CrossRef]
5. Sun, D.X.; Cui, D.L.; Shi, J.T. Hot Cracking and Microstructure of Welding Joint of Magnesium Alloy AZ91D. *Adv. Mater. Res.* **2013**, *753–755*, 435–438. [CrossRef]
6. Ye, H.; Zhang, X.B.; Chang, X.; Chen, R. Microstructures and Properties of Laser Al Alloying on AZ31 Magnesium Alloy. *Adv. Mater. Res.* **2011**, *189–193*, 867–870. [CrossRef]
7. Suo, X.; Guo, X.; Li, W.; Planche, M.-P.; Liao, H. Investigation of Deposition Behavior of Cold-Sprayed Magnesium Coating. *J. Therm. Spray Technol.* **2012**, *21*, 831–837. [CrossRef]
8. Suo, X.; Guo, X.; Li, W.; Planche, M.-P.; Bolot, R.; Liao, H.; Coddet, C. Preparation and Characterization of Magnesium Coating Deposited by Cold Spraying. *J. Mater. Process. Technol.* **2012**, *212*, 100–105. [CrossRef]
9. Li, C.; Li, W.; Liao, H. Examination of the Critical Velocity for Deposition of Particles in Cold Spraying. *J. Therm. Spray Technol.* **2006**, *15*, 212–222. [CrossRef]
10. Pathak, S.; Saha, G.C. Development of Sustainable Cold Spray Coatings and 3D Additive Manufacturing Components for Repair/Manufacturing Applications: A Critical Review. *Coatings* **2017**, *7*, 122. [CrossRef]
11. Ren, Y.Q.; King, P.C.; Yang, Y.S.; Xiao, T.Q.; Chu, C.; Gulizia, S.; Murphy, A.B. Characterization of heat treatment-induced pore structure changes in cold-sprayed titanium. *Mater. Charact.* **2017**, *132*, 69–75. [CrossRef]
12. Wang, Y.; Normand, B.; Mary, N.; Yu, M.; Liao, H. Microstructure and corrosion behavior of cold sprayed SiCp/Al 5056 composite coatings. *Surf. Coat. Technol.* **2014**, *251*, 264–275. [CrossRef]
13. Wang, Y.; Normand, B.; Mary, N.; Yu, M.; Liao, H. Effects of ceramic particle size on microstructure and the corrosion behavior of cold sprayed SiCp/Al 5056 composite coatings. *Surf. Coat. Technol.* **2017**, *315*, 314–325. [CrossRef]
14. Villafuerte, J. Practical Cold Spray Success Repair of Al and Mg Alloy Aircraft Components. *Int. Therm. SPRAY Surf. Eng.* **2010**, *5*, 53–55.
15. Spencer, K.; Fabijanic, D.M.; Zhang, M.-X. The use of Al–Al_2O_3 cold spray coatings to improve the surface properties of magnesium alloys. *Surf. Coat. Technol.* **2009**, *204*, 336–344. [CrossRef]

16. Yoon, S.; Kim, H.; Lee, C. Fabrication of automotive heat exchanger using kinetic spraying process. *Surf. Coat. Technol.* **2007**, *201*, 9524–9532. [CrossRef]
17. Rech, S.; Surpi, A.; Vezzù, S.; Patelli, A.; Trentin, A.; Glor, J.; Frodelius, J.; Hultman, L.; Eklund, P. Cold-spray deposition of Ti 2 AlC coatings. *Vacuum* **2013**, *94*, 69–73. [CrossRef]
18. Rahim, T.A.; Takahashi, K.; Yamada, M.; Fukumoto, M. Effect of Powder Calcination on the Cold Spray Titanium Dioxide Coating. *Mater. Trans.* **2016**, *57*, 1345–1350. [CrossRef]
19. Chang, L.L.; Shang, E.F.; Wang, Y.N.; Zhao, X.; Qi, M. Texture and microstructure evolution in cold rolled AZ31 magnesium alloy. *Mater. Charact.* **2009**, *60*, 487–491. [CrossRef]
20. Yu, M. Elaboration de Composites à Matrice Métallique D'alliages D'aluminium par Projection à Froid. Ph.D. Thesis, Université de Technologie de Belfort-Montbéliard Ecole, Belfort, France, 2013.
21. Sumida, M.; Jung, S.; Okane, T. Solidification Microstructure, Thermal Properties and Hardness of Magnesium Alloy 20 mass% Gd Added AZ91D. *Mater. Trans.* **2009**, *50*, 1161–1168. [CrossRef]
22. Van Steenkiste, T.H.; Smith, J.R.; Teets, R.E.; Moleski, J.J.; Gorkiewicz, D.W.; Tison, R.P.; Marantz, D.R.; Kowalsky, K.A.; Riggs, W.L.; Zajchowski, P.H.; et al. Kinetic spray coatings. *Surf. Coat. Technol.* **1999**, *111*, 62–71. [CrossRef]
23. Suo, X.K.; Guo, X.P.; Li, W.Y.; Planche, M.P.; Zhang, C.; Liao, H.L. Microstructure and wear behavior of SiCp-reinforced magnesium matrix composite by cold spraying. In *Advanced Manufacturing Technology, Pts 1–3, Guangzhou, China, 16–18 September, 2011*; Gao, J., Ed.; TRANS TECH PUBLICATIONS Ltd.: Zurich, Switzerland, 2011; Volume 314–316, pp. 253–258.